Sonar Processing Methods for Reverberation-Limited Undersea Environments

ILKKA KARASALO, MAGNUS LUNDBERG NORDENVAAD,
BERNT NILSSON, PER-AXEL KARLSSON, ELIAS PARASTATES

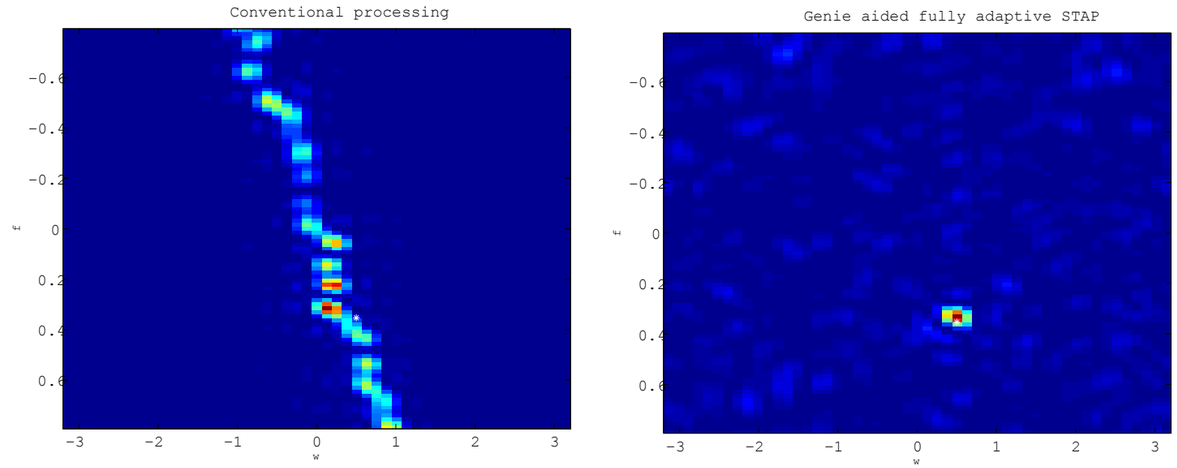

FOI, Swedish Defence Research Agency, is a mainly assignment-funded agency under the Ministry of Defence. The core activities are research, method and technology development, as well as studies conducted in the interests of Swedish defence and the safety and security of society. The organisation employs approximately 1000 personnel of whom about 800 are scientists. This makes FOI Sweden's largest research institute. FOI gives its customers access to leading-edge expertise in a large number of fields such as security policy studies, defence and security related analyses, the assessment of various types of threat, systems for control and management of crises, protection against and management of hazardous substances, IT security and the potential offered by new sensors.

FOI
Defence Research Agency
Defence & Security, Systems and Technology
SE-164 90 Stockholm

Phone: +46 8 555 030 00
Fax: +46 8 555 031 00

www.foi.se

FOI-R--2661--SE Technical report
ISSN 1650-1942 November 2008

Defence & Security, Systems and Technology

Ilkka Karasalo, Magnus Lundberg Nordenvaad,
Bernt Nilsson, Per-Axel Karlsson and
Elias Parastates

Sonar Processing Methods for Reverberation-Limited Undersea Environments

Titel	Sonarmetoder för reverberationsbegränsade undervattensmiljöer
Title	Sonar Processing Methods for Reverberation-Limited Undersea Environments
Rapportnr/Report no	FOI-R--2661--SE
Rapporttyp Report Type	Teknisk rapport Technical report
Sidor/Pages	48 p
Månad/Month	November
Utgivningsår/Year	2008
ISSN	ISSN 1650-1942
Kund/Customer	Försvarsmakten
Forskningsområde Programme area	4. Sensorer och signaturanpassning 4. Sensors and Low Observables
Delområde Subcategory	43 UV-teknik – sensorer 43 Underwater Technology - Surveillance, Target acquisition and Reconnaissance
Projektnr/Project no	E20608
Godkänd av/Approved by	Matts Gustavsson

FOI, Totalförsvarets Forskningsinstitut

Avdelningen för Försvars- och säkerhetssystem

164 90 Stockholm

FOI, Swedish Defence Research Agency

Defence & Security, Systems and Technology

SE-164 90 Stockholm

Sammanfattning

I rapporten presenteras resultat från en studie av lovande metoder vilka har potential att förbättra prestanda för aktiv sonar-system i reverberationsbegränsade miljöer.

Till att börja med har två metoder för blekning av reverberation implementerats och utvärderats med data från simuleringar och från fältförsök. Den optimala sonarmottagaren är formulerad för störningar (reverberation i grunda vatten) som är spektralt vita och en förprocessering som bleker -- eller vitar -- störningarna bör följaktligen kunna ge bättre resultat. Den första metoden bygger på en anpassning av det matchade filtret i sonarmottagaren, som bleker reverberationen. Anpassningen görs för varje avståndslucka med hjälp av ett estimat av reverberationens kovariansmatris. En något bättre detektionsförmåga erhålls med simulerad reverberation i form av rosa brus, men till en mycket hög kostad i form av beräkningar. Den andra metoden bygger på autoregressiv (AR) modellering av reverberationen i en avståndslucka och modellens parametrar används därefter för att bleka reverberationen i nästa avståndslucka. Den här metoden gav väsentligt bättre detektionsprestanda då den applicerades på data från ett fältförsök, och till en rimlig beräkningskostnad.

Vidare, Space-Time Adaptive Processing (STAP) är en lovande signalbehandlingsteknik som ger god undertryckning av spatio-temporala störningar som reverberation och störare. Följaktligen underlättar den detektion av svaga och långsamma mål vars egenskaper ligger nära störningarnas. Den största nackdelen med STAP jämfört med konventionell processering ligger i en betydande ökning av antalet frihetsgrader, vilket leder till stora beräkningskrav och till behov av stora träningsdatamängder. De senare finns inte alltid tillgängliga. I rapporten föreslås en hierarkisk tillvägagång med kraftigt reducerad komplexitet för att komma till rätta med problemen, och vi visar att den ger betydligt bättre prestanda än vanlig STAP för små träningsdatamängder.

Slutligen, syntetisk apertur-sonar (SAS), vilken används i avancerade minjaktssonarer, appliceras här vid lägre frekvenser för övervakningsändamål. SAS-processeringen läggs här till som ett komplement till en konventionell rörlig övervakningssonar med syftet att öka upplösningen i sonarbilden i sonarens rörelseriktning. Det här skulle kunna ge en mer korrekt och detaljerad bild av undervattensmiljön, exempelvis flera mål i högre upplösning, och upptäckt och åskådliggörande av målskuggor i bottenreverberationen. Simuleringar av bevakning under ideala omständigheter, speciellt konstant ljudhastighet (både i rummet och i tiden) och försumbara fel i positioneringen av sonaren visar att bra resultat kan erhållas för användbara avstånd och frekvenser. Andra än ideala omständigheter har också undersökts, exempelvis fel i navigeringsdata för sonaren och flervägsutbredning.

Nyckelord: Reverberationsundertryckning, reverberationsblekning, AR-modellering, aktiv sonar, syntetisk apertur-sonar, SAS, space-time adaptive processing, STAP

Summary

This report presents preliminary results from a study of promising methods with the potential to improve the performance of active sonar systems in reverberation-limited environments.

First, two methods for whitening of reverberation noise have been implemented and studied using simulated and sea trial data. In the first method the matched filter receiver is tuned for each rangebin using an estimate of the reverberation covariance matrix. It is shown to provide better detection performance on a set of simulated data, but at a very large cost in the form of calculations. The second method uses autoregressive (AR) modelling of the reverberation noise, and the AR coefficients are then used to whiten the reverberation in sea trial data. Detection performance was improved significantly using the AR filter, and this was achieved at a fairly low computational cost.

Second, Space-Time Adaptive Processing (STAP) is a promising signal processing technique that offers good mitigation of spatio-temporal interference, such as reverberation and jammers. Hence, it facilitates the detection of weak and slowly moving targets whose properties lie close to the interference characteristics. The major drawback of STAP, compared to conventional processing, is a substantial increase in degrees of freedom. This in turn yields large computational costs and a need of large training data sets which are not always readily available. This report proposes a hierarchical approach to overcome these shortcomings where in each step a decreasing number of sub-problems is solved. In this way, the complexity is greatly reduced compared to standard STAP approaches. Also, since the method combines solutions to sub-problems of smaller dimensionality, the required size of the noise training data set is also greatly reduced. As a result, the derived scheme performs better than standard STAP algorithms for small sample support.

Third, Synthetic Aperture Sonar (SAS) processing, commonly used in advanced mine hunting sonars, is here applied in lower frequency surveillance applications. The SAS processing is added as a complement to the conventional single ping processing of the echoes received by a moving surveillance sonar, with the purpose to significantly increase the azimuthal (along-track) resolution in the sonar image. This could enable a more accurate and informative mapping of the surveyed scene, including higher resolution of multiple targets, detection of target shadows in the bottom reverberation, and resolution of the shapes of such shadows. Simulations made under idealized surveillance conditions, in particular constant (both space- and time-independent) sound speed and negligible errors in positioning of the sonar, indicate that good results can be obtained for relevant distances and frequencies. Less than ideal conditions are also investigated, including effects of errors in navigation data of the sonar and multiple bottom and surface reflections.

Keywords: Reverberation suppression, reverberation whitening, AR modelling, active sonar, synthetic aperture sonar, SAS, space-time adaptive processing, STAP

Contents

1 Introduction

In this report we present signal processing methods aiming to improve the active sonar surveillance in reverberation limited undersea environments. High reverberation levels complicate the detection and classification performance of an active sonar system, particularly in shallow waters like the Swedish archipelagos. The effects of reverberation can be mitigated in many ways, one of which is minimization of the reverberating volume. This can be accomplished through careful selection of sonar waveform [1, 2, 3] and through beamforming of either or both of the transmitter and the receiver [4]. In this report however, we look at several other reverberation mitigation methods. To assess performance, the methods were applied to sample simulated and real seatrial data. The simulated data were created to represent the output of a current sonar system and the experiment dataset was acquired during the BAROC seatrial in 2002 [5]. Note however that the methods studied here are general and there is no reason to assume that they will not apply equally well to data from other sonar systems.

Most traditional processing schemes apply a decoupled approach, i.e. processing is performed either in a spatial-then-temporal or a temporal-then-spatial manner. Focusing on the former approach this means that spatial properties are first addressed using beamforming followed by temporal processing to identify Doppler properties.

In our first investigation we will assess the performance of the optimal detector for the case with a known signal in interfering reverberation and noise [6, 7, 8, 9]. We will consider a spatial-then-temporal approach in which the spatial processing is performed using conventional beamforming. Hence reverberation mitigation is here addressed in the temporal domain only. Basically, the matched filter is prewhitened using an estimate of the interfering reverberation covariance matrix before it is applied to the received data. Since the covariance matrix normally varies with time, the matched filter must be updated continuously yielding a heavy computational workload. As an alternative, whitening has also been performed using autoregressive (AR) modelling of the reverberation data [10, 11], which is also a computationally more efficient procedure.

Extending the above mentioned ideas to address not only temporal properties, but the joint space-time reverberation properties render algorithms that are commonly referred to as Space-Time Adaptive Processing (STAP), see for instance [12] and references therein. Such signal processing techniques are commonly used in radar to enhance the ability to detect targets that might otherwise be obscured by interference, especially in moving platform scenarios where optimal reverberation suppression has to be attacked using a joint approach. STAP is here applied to active sonar in order to mitigate reverberation, specifically targeting scenarios with moving sensor platforms. The major drawback of STAP, compared to more traditional processing approaches, lies in a substantial increase in degrees of freedom see [12]. This potentially yields great computational cost in implementing these techniques along with the need for large training data sets which might be difficult to obtain. Our approach in this report is hence to focus on low-complexity techniques that require only small training data sets.

Finally, Synthetic Aperture Sonar (SAS) processing, commonly used in advanced mine hunting sonars, [13], is here applied at lower frequencies for surveillance applications in order to enhance the capability to classify detected echoes

and to reduce the false alarm probability. The effects of uncertainties concerning the sound velocity profile and the SAS array position on the produced SAS image are studied through simulations.

The layout of this report is as follows. Chapter 1 is this introductory text. Chapter 2 presents the implementation and study of two methods for reverberation prewhitening. Section 2.1 discusses prewhitening with the conventional matched filter detector and in section 2.2 a whitening method based on AR modelling of the reverberation is presented. Chapter 3 presents results from applying low-complexity techniques to STAP processing. In chapter 4 SAS processing is applied at lower frequencies to reduce the false alarm probability. The report is concluded in chapter 5.

2 Reverberation whitening

2.1 Covariance-tuned matched filter

The active sonar detection case is often processed using hypothesis testing, where one hypothesis is that we have only noise in our observation and where the other hypothesis is that we also have a signal in the form of a target echo present. Using the basic model where the target is a point-reflector, the received signal is a delayed and attenuated version of the emitted pulse or ping. Since we do not generally have access to the a priori probabilities it is common practice to use the Neyman-Pearson criterion [6, 7, 14] which only requires the probability distributions of the signal and noise respectively.

In the Neyman-Pearson detector a likelihood ratio is used to signal a detection. The probability distribution of a certain observation $\mathbf{x}$ of the received signal under each of the two hypoteses and their quotient is formed, i.e.

$$\Lambda = \frac{p_1(\mathbf{x})}{p_0(\mathbf{x})} \underset{H_0}{\overset{H_1}{\gtrless}} \beta \tag{2.1}$$

where the suffix 0 corresponds to hypothesis H_0 (noise only) and suffix 1 corresponds to hypothesis H_1 (target echo is present). Given an observation $\mathbf{x}$ we choose H_1 when $\Lambda \geq \beta$ and H_0 otherwise.

In the ambient noise-limited case we model an active sonar as operating in the presence of additive white Gaussian noise only. This is a reasonable model when the sonar is operated in deep water, i.e. where any reflecting surfaces, apart from the point-reflector-like target, are far from the sonar. The hypotheses for the received signal length-N vector $\mathbf{x}(t)$ here are

$$H_0 \quad : \quad \mathbf{x}(t) = \mathbf{n}(t) \tag{2.2}$$

$$H_1 \quad : \quad \mathbf{x}(t) = \mathbf{s} + \mathbf{n}(t) \tag{2.3}$$

where $\mathbf{s}$ is the emitted signal, and $\mathbf{n}(t)$ is the noise contribution to the received signal at time instant t. To be able use the detection criterion in equation (2.1), we need the probability density functions for the received signal under both hypotheses. Under hypothesis H_0 we use the multivariate complex normal (Gaussian) distribution to obtain

$$p_0(\mathbf{x}) = \frac{\exp(-\mathbf{x}^H \mathbf{R}_n^{-1} \mathbf{x})}{(\pi)^N |\mathbf{R}_n|} \tag{2.4}$$

where $\mathbf{R}_n$ is the noise covariance matrix. Using the same distribution under H_1 for $\mathbf{x} - \mathbf{s}$, we obtain

$$p_1(\mathbf{x}) = \frac{\exp(-(\mathbf{x} - \mathbf{s})^H \mathbf{R}_n^{-1} (\mathbf{x} - \mathbf{s}))}{(\pi)^N |\mathbf{R}_n|} \tag{2.5}$$

It is now possible to form the likelihood ratio

$$\Lambda = \frac{p_1(\mathbf{x})}{p_0(\mathbf{x})} = \exp\left\{ \left(\mathbf{s}^H \mathbf{R}_n^{-1} \mathbf{x} + \mathbf{x}^H \mathbf{R}_n^{-1} \mathbf{s} - \mathbf{s}^H \mathbf{R}_n^{-1} \mathbf{s} \right) \right\} \tag{2.6}$$

Here the third term in the exponent does not depend on the received data ($\mathbf{x}$) and can therefore be omitted, or more formally, be incorparated into the

threshold β. Using a similar argument, the first and second terms are transposes of eachother and it suffices to use one of them. Also, since $\exp(\cdot)$ is a monotonically increasing function in its argument, it is sufficient to study the argument itself. Consequently, an equivalent form of the Neyman-Pearson test in (2.1) becomes

$$\Lambda' = \mathbf{s}^H \mathbf{R}_n^{-1} \mathbf{x} \underset{H_0}{\overset{H_1}{\gtrless}} \beta'. \tag{2.7}$$

In a real application the signal part $\mathbf{s}$ of the received signal is seldom known exactly. Often only its shape is known while its amplitude α is unknown. Hence a more correct formulation of the received signal under hypothesis H_1 would be

$$H_1 \ : \ \mathbf{x}(t) = \alpha \mathbf{s} + \mathbf{n}(t) \tag{2.8}$$

and we note that the distribution under hypothesis H_1 is thus also unknown. One way to attack this problem is to estimate α with a maximum likelihood method and then use the estimate $\hat{\alpha}$ as if it was the true amplitude in eqn. (2.8). This procedure is known as the generalized likelihood ratio test (GLRT). Even though the GLRT is only asymptotically optimal it performs well in many real applications. For this case the test in eqn. (2.7) becomes

$$\Lambda'' = |\mathbf{s}^H \mathbf{R}_n^{-1} \mathbf{x}|, \tag{2.9}$$

see for example [15] and references therein.

A commonly used assumption is that the additive noise is spectrally white and independent. The covariance matrix may the be written $\sigma^2 \mathbf{I}$ where σ^2 is the noise variance and $\mathbf{I}$ is the identity matrix. The noise variance may be set to 1 without loss of generality and the test statistic for this case becomes

$$\Lambda''' = |\mathbf{s}^H \mathbf{x}| \tag{2.10}$$

which is the output of a traditional matched filter or replica correlator. Thus the matched filter corresponding to eqn. (2.10) is the optimal detector for the case when the noise component is white and independently distributed. Conversely, if this is not true, the above result means we should be able to have better detection performance if we compensate the replica s with the inverse of the current noise covariance matrix $\mathbf{R}_n^{-1}$. The latter is seldom known, so normally an estimate will have to be used.

The reverberation-limited case is handled analogously by considering the signal $\mathbf{s}$ to be deterministic and the reverberation to be stochastic. The hypotheses for this case are [8],

$$H_0 \ : \ \mathbf{x}(t) = \mathbf{c}(t) + \mathbf{n}(t) \tag{2.11}$$

$$H_1 \ : \ \mathbf{x}(t) = \mathbf{s} + \mathbf{c}(t) + \mathbf{n}(t) \tag{2.12}$$

where $\mathbf{c}$ is a reverberation or clutter term. If we assume that this term is also Gaussian distributed and uncorrelated with the ambient noise term [8, 16, 11], we may treat $\mathbf{c}$ and $\mathbf{n}$ together as a Gaussian process with a covariance matrix that is the sum of the individual covariance matrices, $\mathbf{R}_c + \mathbf{R}_n$. In the following, this aggregate covariance matrix will be denoted $\mathbf{R}_n$. Under these assumptions the optimal processor is the same as in the noise-limited case, but with a different covariance matrix.

In order to assess the value of reverberation whitening a simulation was performed. Pink coloured (i.e. where the power spectral density is proportional to the reciprocal of the frequency, $1/f$) Gaussian noise was generated and was used to simulate reverberation in the output of a beamformer. A point target echo was added in the form of a 200 ms linear frequency-modulated (LFM) chirp. The center frequency of the chirp was 1500 Hz and the bandwidth 1000 Hz.

This output beam signal was passed through the matched (to the LFM signal) filter of eqn. (2.7) to obtain pulse compression. One hundred range-bins, centered at the range-bin containing the target echo, of the matched filter output were chosen for presentation. The matched filter output was also normalized so that the target echo was equal to 1.

Sample covariance matrices were calculated for each range-bin of the beamformer output and finally averages over 10 range-bins were used as the estimate of the covariance matrix $\mathbf{R}_n$ in eqn. (2.7). The estimate $\hat{\mathbf{R}}_n$ was then applied to the range-bin immediately following the interval of range-bins used for the estimate.

The pulse length of the chirp in the complex baseband (i.e. the length of the matched filter) was 200 samples, and consequently the covariance matrices were of size 200×200. Since the covariance matrix estimates were based on only 10 range-bins each, some sort of regularization had to be performed. Here we used diagonal loading, i.e. the following matrix was added to each covariance matrix estimate

$$k\sigma_n^2\mathbf{I},$$

where the constant k was set to 2 and where σ_n^2 is the variance of the generated pink noise and $\mathbf{I}$ is an identity matrix of size 200×200. The constant k was varied to some extent, but its value did not prove important for this simple simulation.

For comparison the reverberation whitening receiver was also compared to the more traditional active sonar receiver of eqn. (2.10), where the matched filter is fixed, i.e. does not change with time (range-bin). The output of the matched filters on the range interval of interest (where the target is located) is found in figure 2.1.

Local maxima (peak amplitudes) on both sides of the target echo in figure 2.1 (but excluding the target echo itself) and their mean values over 100 pink noise realisations were found and compared, with and without whitening. In this simulation the mean peak level was decreased by approximately 17 % with whitening compared to without whitening. For a given detection probability (i.e. for a given detection threshold) this means fewer false alarms or a decreased false alarm probability.

Computationally the use of an inverse covariance matrix estimate for reverberation suppression can be very costly, especially for long sonar pulses. Since the matched filter is essentially the emitted signal itself, it will be equally long and the corresponding covariance matrix will be the square of that length. This means that a very large set of data must be available in order to estimate $\mathbf{R}_c$.

The covariance whitening was also tested on experiment data. The data we had at hand were recorded during the BAROC sea trial in the Baltic Sea in 2002 [5, 17]. The BAROC sea trial was a collaboration between the FOI and the FWG of Germany. In the particular run used here, a monostatic setup was used. An omnidirectional transmitter emitted a 2 s linear frequency-modulated (LFM) pulse with a center frequency of 1.5 kHz and a bandwidth of 1 kHz. The receiving antenna was a 32-element uniform linear array (ULA) in a horizontal

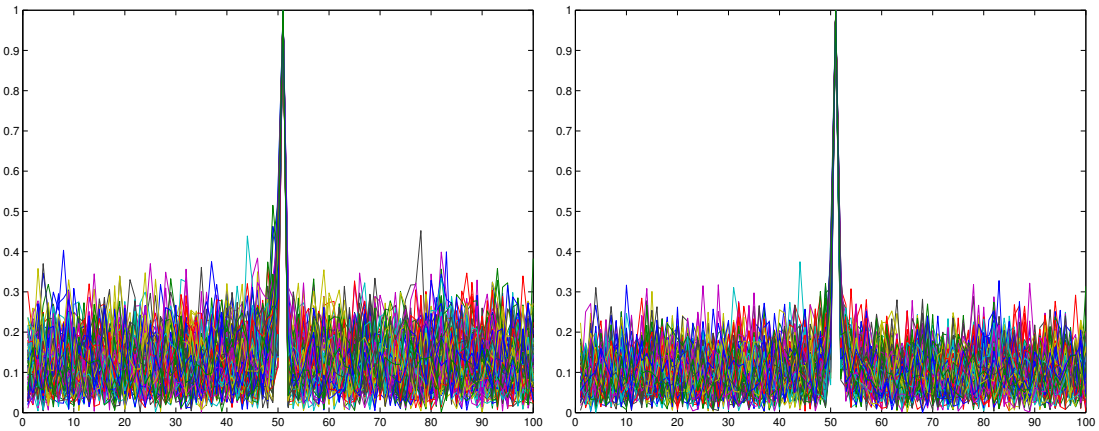

Figure 2.1: Matched filter output without (left) and with (right) reverberation whitening for 100 pink noise reverberation realisations. To the left the matched filter is fixed, i.e. it does not change for each range-bin. To the right the matched filter is updated for each range-bin with an estimate of the covariance matrix from 10 previous range-bins. A 17 % decrease of the mean peak level on either side of the target was found.

arrangement. The design frequency of the array was 3 kHz. The setup was static in that neither the transmitter nor the receiver was moving.

The data were beamformed and the broadside beam was selected for further processing and display. The covariance matrix $\mathbf{R}_c$, was estimated from range-bins outside the one under observation, and the matched filter was updated for each range-bin, before it was being applied to the broadside beam data.

With a baseband sampling rate of 1 kHz the matched filter for this data set will be 2000 samples long and the covariance matrix a huge 2000×2000 samples. Consequently we were expecting problems in estimating this matrix well enough to enjoy better detection performance, and this also proved to be the case. We were not able to see any benefits from the whitening on this dataset, probably due to the very large number of samples needed to get a good estimate of the covariance matrix and that the reverberation was not constant during that time. In the next section however, we shall see that autoregressive modelling of the reverberation will provide significant improvements for the BAROC sea trial data.

2.2 Autoregressive filtering

We have seen one example of the advantages of reverberation whitening. We observe that true whitening can only be performed if $\mathbf{R}_n$ is known. In other cases approximations have to be made. The solution in section 2.1 is one such appproach. In fact approximate whitening can be performed in many different ways, and a relatively low-complex solution was presented in [11]. Here the whitening is based on an autoregressive (AR) model of the reverberation noise in each beam signal. The use of an AR model is motivated by the fact that the reverberation spectrum depends heavily on the underwater environment and often changes with time. Consequently, a prewhitener must be able to model the reverberation spectrum using only small sets of data and the AR model is very good at this [10].

The reverberation noise component is modelled as

$$n_t = -\sum_{k=1}^{p} a_k n_{t-k} + \epsilon_t \tag{2.13}$$

where a_k are the AR coefficients, p is the AR filter order and ϵ_t is a white noise process that drives the AR process. The AR model coefficients are estimated for each rangebin and the inverse, or whitening, FIR filter is then

$$\hat{A}(z) = 1 + \sum_{k=1}^{p} \hat{a}_k z^{-k}. \tag{2.14}$$

The whitening filter is subsequently used to inverse filter the reverberation data in the following rangebin. Under the assumption that the reverberation colour is fairly constant from one rangebin to the next, there should be a signifigant decrease of the reverberation levels from the whitening. The whitening filter is also applied to the matched (to the sonar waveform) filter in the sonar receiver before the matched filter is applied.

Once again one ping of the BAROC data described in section 2.1 was beamformed and the broadside beam was chosen for whitening and presentation. For reference, a target echo was added to the raw data at a range corresponding to rangebin 353. The beam signal was divided into rangebins of the same size as the sonar pulse, here 2000 samples, and a rangebin step size of 20 samples was used (i.e. the rangebin overlap was 1980 samples). An AR model of order 10 was fit to the data in one rangebin and the inverse filter was applied to the following rangebin and to the matched filter.

The results of the autoregressive whitening are shown in figure 2.2 for the full observation time of one ping (upper two graphs) and for the range-interval around the added target echo at range-bin 353 (lower two graphs). Relative to the target echo peak at rangebin 353, the output levels are in general significantly reduced. Hence, the detection threshold could be lowered with no accompanying increase of false alarms as a result.

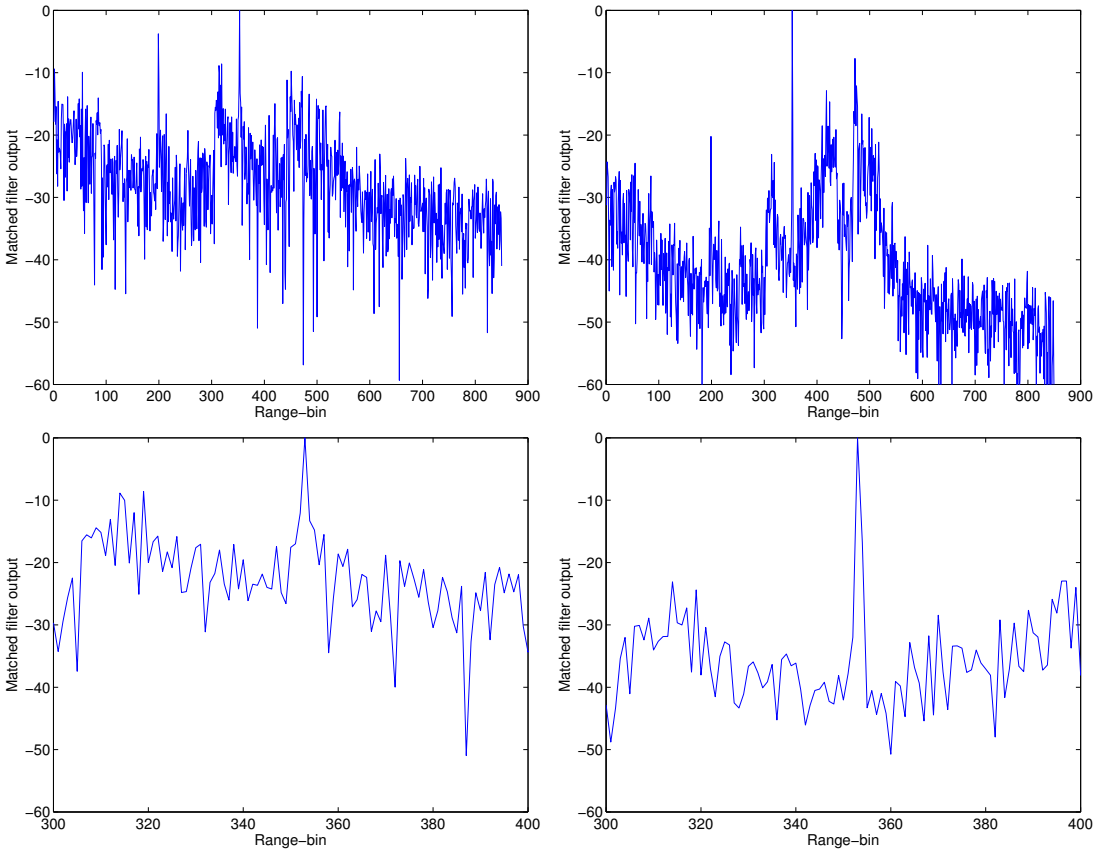

Figure 2.2: Matched filter output without (left) and with (right) reverberation whitening using autoregressive (AR) modelling of an active sonar data set from the BAROC sea trial. The lower two graphs show a zoom of the upper two graphs for the rangebin interval 300-400. To the left the matched filter is fixed, i.e. it does not change for each rangebin. To the right the matched filter is updated for each rangebin with an autoregressive whitening filter and is then applied to data from the next rangebin after this has been prewhitened. After normalization to the added target at rangebin 353, it is evident that the reverberation in adjacent rangebins has been significantly reduced.

3 Space-Time Adaptive Processing (STAP)

The primary target of an under water surveillance system is to detect targets in the presence of noise, reverberation and jammers. The task becomes particularly challenging if the surveillance is performed from a moving platform since the platform motion renders self induced Doppler spread of the reverberation. However, the reverberation will in this case contain structure since a certain bearing can be related to a certain doppler shift [18, 12, 19].

The purpose of Space-Time Adaptive Processing (STAP), [12, 19] is to address this feature by generalizing the approach taken in Section 2. Considering a joint space-time approach enables mitigation of subspace interference in the spatio-temporal domain, contrary to subspace mitigation in the temporal or spatial domains alone. Such a strategy therefore has its evident advantages since the effect on reverberation caused by platform motion have exactly those properties.

The major drawback of STAP lies in substantial increase in degrees of freedoms, compared to conventional processing. This potentially yields great computational cost in implementing these techniques along with the need of large training data sets which might be difficult to obtain.

3.1 Space-Time Data Model

Basically the idea of STAP is to generalize the results considered in Section 2. However, instead of considering already beamformed data and only consider temporal processing, we here take a space-time approach. Assuming that the system under consideration transmits a CW-pulse and that a target is present in a specific range bin, the discrete-time baseband array data can be modeled as

$$\mathbf{x}(k) = s\ \mathbf{a}(\phi)e^{j\omega k} + \mathbf{n}(k), \quad k = 1\ldots, M, \tag{3.1}$$

for time index k. Here s is the complex amplitude of the target, ω is the Doppler shift due to relative motion between the platform and the target, $\mathbf{a}(\phi)$ is the array response of the N-element array, and $\mathbf{n}(k)$ contains the contributions from reverberation, noise, and jamming signals.

By stacking the M array measurements into a $NM \times 1$ space-time snapshot, we can express the measured data as

$$\mathbf{x} = \begin{bmatrix} \mathbf{x}(1) \\ \mathbf{x}(2) \\ \vdots \\ \mathbf{x}(M) \end{bmatrix} = s\mathbf{r}(\phi, \omega) + \mathbf{n} \tag{3.2}$$

Above $\mathbf{n}$ denotes the disturbance obtained by stacking the noise and interference components $\mathbf{n}(k)$ and $\mathbf{r}(\phi, \omega)$ denotes the spatio-temporal array response

$$\mathbf{r}(\phi, \omega) = \mathbf{d}(\omega) \otimes \mathbf{a}(\phi)$$

where

$$\mathbf{v}(\omega) = [1\ e^{j\omega}\ e^{j2\omega}\ \ldots\ e^{j(M-1)\omega}]^T$$

and $\otimes$ is the Kronecker product.

3.2 STAP processing

Similar to (2.9), in STAP the purpose is to design a space-time beamformer, $\mathbf{w}(\phi, \omega)$, which applied to the measured data $\mathbf{x}$, renders the angle-Doppler spectrum

$$P(\phi, \omega) = \left| \mathbf{w}^H(\phi, \omega)\mathbf{x} \right|^2 . \tag{3.3}$$

Considering that the underlying task is to mitigate interference and noise, a natural design criterion for $\mathbf{w}(\phi, \omega)$ is to maximize the signal-to-interference plus noise ratio (SINR). Under such an approach the spatio-temporal beamformer is given as

$$\mathbf{w}(\phi, \omega) = \mathbf{R}_n^{-1}\mathbf{r}(\phi, \omega) \tag{3.4}$$

where $\mathbf{R}_n$ is disturbance covariance matrix

$$\mathbf{R}_n = E\left(\mathbf{n}\mathbf{n}^H\right),$$

see [20, 12]. We also note from (2.9) that this solution can be interpreted through the Generalized Likelihood Ratio Test (GLRT) framework. However, as described in section 2, $\mathbf{R}_n$, is rarely known a priori but has to be estimated by some means. As described in [12, 19] and Section 2 the most common way is here to use secondary data collected from adjacent range bins. Let $\mathbf{x}_l, l = 1, \ldots, L$ denote these data. Means to incorporate partial prior knowledge regarding $\mathbf{R}_n$, using physical models, is also a very active field in the research community, see [21] and references therein.

In most applicable scenarios, $L << MN$ whereby the standard covariance matrix estimator

$$\hat{\mathbf{R}}_n = \frac{1}{L}\sum_{l=1}^{L} \mathbf{x}_k \mathbf{x}_k^H, \tag{3.5}$$

cannot be used since $\hat{\mathbf{R}}_n$ becomes singular with probability one. Nevertheless, since (3.5) is a sufficient statistic for $\mathbf{R}_n$ it is often a natural component in most STAP solutions.

Perhaps the most common strategy is to employ diagonal loading and use a covariance matrix estimate on the form

$$\hat{\mathbf{R}}_n^{\alpha} = \hat{\mathbf{R}}_n + \alpha\mathbf{I}, \tag{3.6}$$

see [22]. $\mathbf{I}$ is here the identity matrix. Although slightly ad-hoc, diagonally loaded solutions tend to work well in many practical application. In fact, diagonally loaded solutions have some theoretical motivation; such solutions arises by imposing a white noise gain constraint [23] or by considering array response modeling errors [24]. The main difficulty in applying a diagonally loaded solution is to assign the design parameter α. Rules of thumb exist but few techniques to obtain α from data exist. Perhaps the most theoretically sound approach was given in [25] in which an empirical Bayesian strategy was used to obtain α as

$$\alpha = \frac{1}{L}\arg\max_{\gamma} \frac{\gamma^{p^2}}{|\mathbf{X}\mathbf{X}^H + \gamma\,\mathbf{I}|^{L+p}}, \tag{3.7}$$

where $p = NM$ and $\mathbf{X} = [\mathbf{x}_1\ \mathbf{x}_2\ \ldots\ \mathbf{x}_L]$.

By noting that the main difficulty relates to the fact that the amount of training data, L, is usually relatively small compared to the underlying dimensionality of the problem, an alternative approach is to non-adaptively reduce the dimensionality. Such methods are usually referred to as beamspace transforms. Through dimension reduction these techniques impose constraints on the structure of $\mathbf{R}_n$. The desirable consequence of this is that the degrees of freedom that must be estimated from secondary data is reduced and that the computational complexity decreases. The drawback is inherently that some of the adaptivity vanishes, due to the non-adaptive dimension reduction.

In recent years much effort have therefore been put into strategies to find reduced rank solutions in which the dimension reduction is performed in an adaptive fashion; in other words finding dimension reduction techniques that depend on the interference characteristics. Perhaps the most commonly suggested alternative is to use the Multistage Wiener Filters (MWF) as suggested in [26, 27] which to-date is considered to be state-of-the art in STAP processing. Since this strategy was first developed, it has in later work been established that the rank k MWF filter is equivalent to the k^{th} iteration in a conjugate gradient solution [28] to the systems of linear equations,

$$\hat{\mathbf{R}}_n \mathbf{w}(\phi, \omega) = \mathbf{r}(\phi, \omega),$$

see [29] and references therein. Thus we can describe its construction procedure as follows; We start by initializing the recursion using the initial filter vector

$$\mathbf{w}_0 = \mathbf{r},$$

along with an initial search direction $\mathbf{d}_0 = \mathbf{g}_0$. Hence, we initialize the filter with the conventional processor[1]. We have here dropped the dependence on (ϕ, ω) for notational convenience. The vector $\mathbf{g}_0 = \mathbf{r} - \hat{\mathbf{R}}_n \mathbf{w}_0$ is here the initial (negative) gradient vector. Throughout the recursion, the conjugate gradient solution, at iteration k, generates the approximation

$$\mathbf{w}_k = \mathbf{w}_{k-1} + \mathbf{d}_{k-1}\alpha_{k-1}, \tag{3.8}$$

where the step size $\alpha_{k-1} = ||\mathbf{g}_{k-1}||^2 / \, \mathbf{d}_{k-1}^H \hat{\mathbf{R}}_n \, \mathbf{d}_{k-1}$is chosen to optimize the amount of updating along direction $\mathbf{d}_k$, so that the quadratic objective function decreases monotonically. $||\cdot||$ is the euclidean norm, i.e. $||\mathbf{g}|| = \sqrt{\mathbf{g}^H \mathbf{g}}$. Accordingly, the gradient vector is updated as

$$\mathbf{g}_k = \mathbf{g}_{k-1} - \alpha_{k-1} \hat{\mathbf{R}}_n \mathbf{d}_k.$$

Subsequential search directions are chosen as R-conjugate directions:

$$\mathbf{d}_k = \mathbf{g}_k + \frac{||\mathbf{g}_k||^2}{||\mathbf{g}_{k-1}||^2} \mathbf{d}_{k-1}$$

where $\mathbf{d}_k^H \hat{\mathbf{R}}_n \mathbf{d}_m = 0$ for $k \neq m$. At iteration k, we note the following, see also [29].

- The gradients $\mathbf{g}_1, \ldots, \mathbf{g}_k$ turn out an orthogonal basis for the Krylov subspace

  $$\mathcal{K}_k(\hat{\mathbf{R}}_n, \mathbf{r}) = < \mathbf{r}, \hat{\mathbf{R}}_n \mathbf{r}, \ldots, \hat{\mathbf{R}}_n^{k-1} \mathbf{r} >$$

  where $< \mathbf{a}_1, \ldots, \mathbf{a}_k >$ denotes the span of the vectors $\mathbf{a}_1$ through $\mathbf{a}_k$.

[1] If $\mathbf{w}(\phi, \omega) = \mathbf{r}(\phi, \omega)$ the resulting spectrum equals $P(\phi, \omega) = |\mathbf{r}(\phi, \omega)^H \mathbf{x}|^2$. This is the conventional processor as noted in eq. (2.10).

- The directions $\mathbf{d}_1, \ldots, \mathbf{d}_k$ turn out a non-orthogonal basis for $\mathcal{K}_k(\hat{\mathbf{R}}_n, \mathbf{r})$, but the directions are $\hat{\mathbf{R}}_n$-conjugate.

Now, studying (3.8) we note that the resulting filter at iteration k can be regarded as a linear combination of the included direction vectors. Hence, at iteration k the conjugate gradient approach yields a solution which is guaranteed to lie in the rank k subspace $\mathcal{K}_k(\hat{\mathbf{R}}_n, \mathbf{r})$.

The iterations, for any $\hat{\mathbf{R}}_n$, will converge in at most MN steps, yielding the fully adaptive solution. However, for many problems good results are achieved much earlier than that since the convergence properties basically depend on the eigenvalue structure of $\hat{\mathbf{R}}_n$. The procedure is, in fact, guaranteed to converge in l steps where l is the number of distinct eigenvalues of $\hat{\mathbf{R}}_n$, see for instance [30]. Since the interference most often exhibits low-rank structure, in the ideal case with $\mathbf{R}_n$ known, the procedure would thus converge in at most the rank of the interference plus one iterations, where the plus one accounts for the noise eigenvalue. In an application where $\hat{\mathbf{R}}_n$ is used in place of $\mathbf{R}_n$, however, eigenvalue separation in (3.5) renders the number of distinct eigenvalues to equal $\min(MN, L)$ with probability one, see [25]. However, by stopping the procedure after an appropriate number of iterations (basically equaling the rank of the interference plus one) the ill-conditioning and hence the noise enhancement properties of the full-adaptive STAP can be avoided.

We note that this technique produces an implicit dimension reduction that depends on the underlying characteristics, $\hat{\mathbf{R}}_n$, of the interference, this since $\mathbf{w}_k \in \mathcal{K}_k(\hat{\mathbf{R}}_n, \mathbf{r}(\phi, \omega))$. In addition, we note that the dimension reduction is angle-Doppler dependent. In most aspects the latter property is a desired one since the rank reduction take the specific probing parameters (ϕ, θ) into account. However, from a computational perspective this is challenging since it requires the rank reduction to be performed for each individual set of (ϕ, ω). Thus, if we desire to image the whole (ϕ, ω)-plane this yields highly complex solutions. So far, this property has attracted little attention in the research community. In fact, MWF-STAP, or equivalently Conjugate Gradient (CG) STAP is often referred to as a low-complex solution. This is only true if we consider recovering signal energy along very few directions. In fact, in most cases a MWF/CG approach would yield a more complex implementation than a diagonally loaded solution despite the fact that it requires matrix inversion.

To address the shortcomings of the CG approach we return to the basic problem formulation. We note that our desire, in essence, is to approximate

$$\mathbf{r}^H(\phi, \omega)\mathbf{R}_n^{-1}\mathbf{x}, \tag{3.9}$$

see (3.3). The conventional CG-STAP procedure replaces $\mathbf{R}_n^{-1}$ with $\hat{\mathbf{R}}_n^{-1}$ and finds a low-rank approximation to $\mathbf{w}(\phi, \omega) = \hat{\mathbf{R}}_n^{-1}\mathbf{r}(\phi, \omega)$. The computational expense occurs since the low-rank filter $\mathbf{w}_k(\phi, \omega)$ has to be derived for each set of probing parameters (ϕ, ω). Meanwhile we note that (3.9) is symmetrical in $\mathbf{r}(\phi, \omega)$ and $\mathbf{x}$. Hence, in order to avoid having to find the low-rank filter for each set of probing parameters, an alternative is to run the conjugate gradient algorithm against $\mathbf{x}$ instead of $\mathbf{r}^H(\phi, \omega)$, i.e., by studying the spectrum

$$P_{MCG}(\phi, \omega) = |\mathbf{r}^H(\phi, \omega)\mathbf{y}_k|^2 \tag{3.10}$$

where $\mathbf{y}_k$ is the rank k solution to the system of linear equations

$$\hat{\mathbf{R}}_n\mathbf{y} = \mathbf{x}.$$

We refer to this as the *Modified Conjugate Gradient* solution. $\mathbf{y}_k$ can hence be interpreted as a rank k attempt to remove the interference contained in $\mathbf{x}$. The

advantage is of course that we only need to run the conjugate gradient iteration once, irrespective of probing parameters. The disadvantage is naturally that it will not yield probe dependent rank reduction. However, we suspect that the downside of this is limited since the convergence properties of the conjugate gradient scheme basically depends on the eigenvalue structure of $\hat{\mathbf{R}}_n$. Hence we suspect and hope to reach similar performance with significant reduction in computational complexity.

3.3 Evaluations

To investigate the promise of the various STAP techniques for underwater surveillance purposes we will study a scenario which uses a half wavelength spaced N=31 element flanked uniform linear array. For such a scenario the array response is given by

$$\mathbf{a}(\phi) = [1 \; e^{-j\pi \sin\phi} \; e^{-j\pi 2 \sin\phi} \; \ldots \; e^{-j\pi 30 \sin\phi}]^T.$$

The transmitted signal is a 20 ms CW pulse at 25 kHz. Furthermore, it is assumed that the receiver demodulates and downsamples the signal to 1 kHz sampling rate. Hence, in the discrete-time model given above this yields $M = 20$ samples in time, overall generating a scenario with dimensionality $NM = 610$. It is assumed that the sensor platform moves with speed 3 m/s which will render self induced space-time dependent reverberation. The target of interest is located at 0.35 radians with respect to broadside. Furthermore, the target is moving with a heading of 45 degrees compared to that of the sensor platform. This will generate an effective target Doppler shift of 80.5 Hz with 1425 m/s sound propagation or 0.51 radians in the discrete-time model. In conclusion, the target parameters are $\phi = 0.35$ and $\omega = 0.51$. The scenario is summarized and illustrated in Fig. 3.1. Our focus is on reverberation limited scenarios so throughout our simulations the target is modeled to be 20 dB stronger than the background noise.

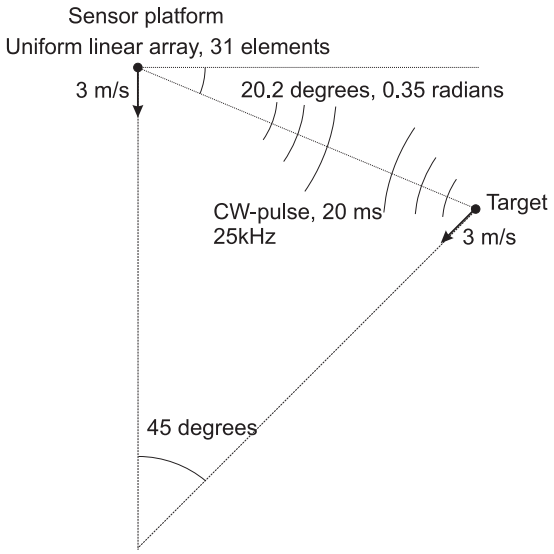

Figure 3.1: Surveillance scenario considered in the STAP evaluations

Two different means to model the signal propagation will be investigated. First, a case in which both the signal and the reverberation is modeled as plane

wave point sources will be studied. Subsequently a case in which the signal propagation is modeled through ray-tracing will be investigated.

3.3.0.1 Plane-wave point reverberation

To model the induced reverberation, we consider 20 point sources quasi-randomly distributed within the Doppler-ridge created by the platform motion. The reverberation is between 2-3 dB stronger than the desired source target.

In Figure 3.2(a) we observe the angle-Doppler spectrum for non-adaptive conventional processing. We specifically note the effect of the structured reverberation, which over-clouds the contribution of the desired target. In Figure 3.2(a) the location of the desired target is indicated with the white mark. In contrast, Figure 3.2(b) illustrates the angle-Doppler spectrum for genie aided STAP, i.e., fully adaptive STAP using the known interference covariance matrix $\mathbf{R}_n$. Naturally, such a solution is not possible to implement in practice since $\mathbf{R}_n$ is not known, however, it serves as a reference and shows the improvements that are possible using an adaptive space-time approach. In 3.2(b), the desired target is clearly visible.

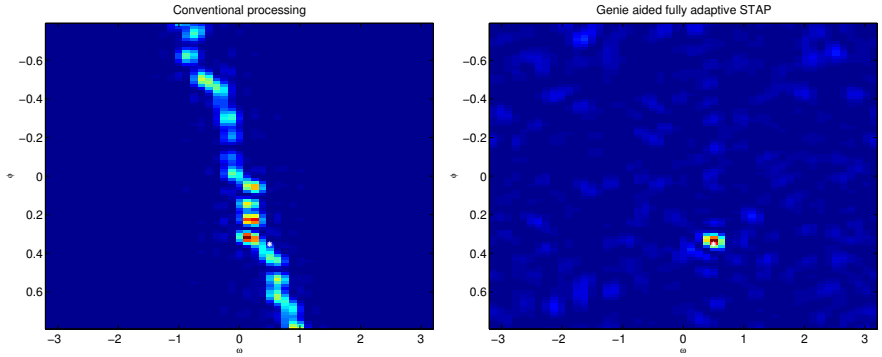

Figure 3.2: From left to right (a)-(b): (a) Angle-Doppler spectrum of conventional processing. The true position of the target is indicated using the white mark. (b) Angle-Doppler spectrum of genie-aided STAP.

As mentioned, the performance of STAP is mainly determined by the ability to characterize the interference using limited amount of training samples. Therefore the purpose is here to investigate the various STAP algorithms in the case of small sample support, in this case $L = 64 << MN$. Three different STAP algorithms will be considered, namely CG-STAP in (3.8), MCG-STAP in (3.10), and diagonally loaded STAP where the regularized covariance matrix estimate in (3.6) and (3.7) is used in place of $\mathbf{R}_n$ in (3.4). For the conjugate gradient based methods results are shown for the rank-22 implementations. The results are given in Figure 3.3.

Looking at the results in Fig. 3.3 we note that all methods show similar and adequate performance. The desired target is clearly visible in all three cases. In fact, the performance is only slightly worse than that of the genie-aided processor in Fig. 3.2b for which the characteristics of the reverberation were perfectly known. Studying the computational efforts in deriving these solutions we however note large differences. The CG-based solution required in the order of 520 time units to compute, the diagonally loaded solution required 33 time units to compute while the modified CG-solution required 0.39 time units. This should be compared to the computational efforts required to find the conventional spectrum in Fig. 3.2a which was 0.22 time units. Hence,

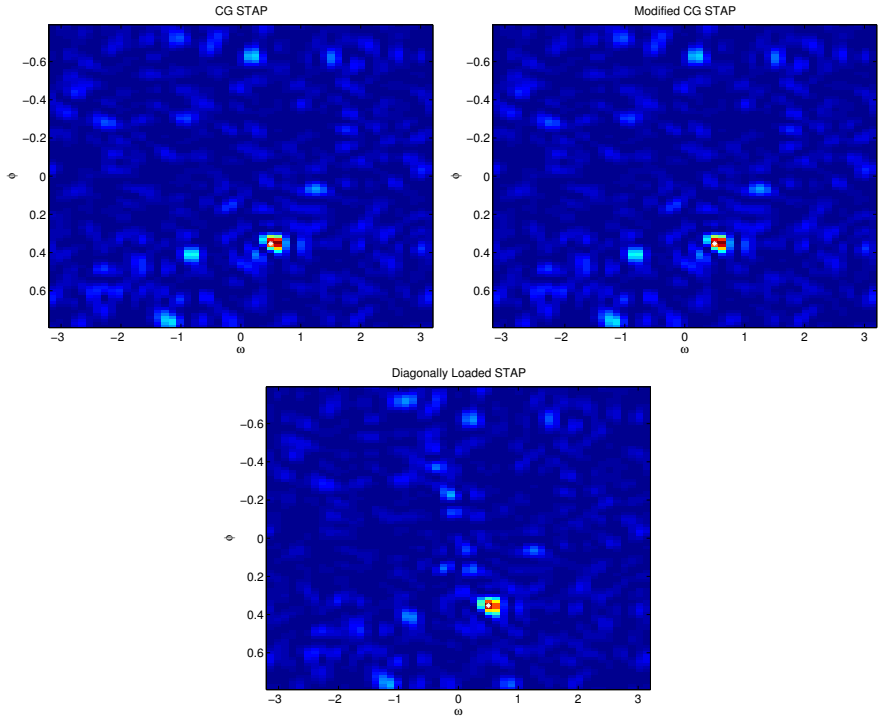

Figure 3.3: From left to right and top to bottom(a)-(c): (a) Angle-Doppler spectrum for CG-STAP. (b) Angle-Doppler spectrum for MCG-STAP. (c) Angle-Doppler spectrum for diagonally loaded STAP. The true position of the target is indicated using the white mark.

in low-rank situations where the secondary data carries sufficient information regarding the reverberation characteristics, the modified conjugate gradient solution appears to offer adaptive performance at similar computational cost compared to the conventional processor.

3.3.0.2 Reverberation through Ray-tracing

The investigated procedures is also tested using time-series generated with the wave-propagation model RAYLAB [31, 32]. The purpose is two-folded. First, we would like to investigate the robustness of the technique to non-ideal propagation. Second, we would like to study how accurately adjacent range bins can characterize the reverberation in the range bin under consideration. Caution is however pointed out since real data i ultimately required in order to accurately assess the performance of the studied techniques.

The simulator RAYLAB is based on ray-tracing [33] and utilizes a layered environment with range independent parameters. The source, the receiver and the target are all situated at a depth of $40\,m$ and the water depth is $60\,m$. Pertinent properties of the sound propagation are summarized in Table 3.1. The target is located 4400 m from the sensor platform, and data corresponding to ranges 4000-4380 and 4440-4800 m are employed as secondary data, i.e., used to estimate $\hat{\mathbf{R}}_n$. Furthermore, the reverberation is here approximately 4dB stronger than the target. Otherwise, the underlying scenario is identical to the one used above.

The results are seen in Fig. 3.4. Again, we notice the Doppler ridge in the conventional spectrum which interferes the target signature. Also, we note

that the adaptive processors are highly successful in mitigating the reverberation. Keeping in mind the the complexity of the modified conjugate gradient technique is just about twice that of the conventional processor in a direct implementation, it is definitely an attractive methodology in active underwater sensing.

The investigated scenario considered a stationary environment in the sense that all environmental parameters such as sound speed profile, bottom characteristics, and water depth were all constant. Since the effectiveness of STAP basically depends on the amount of secondary data that can carry information regarding the cell under investigation, such an assumption favor STAP implementations. In order to fully investigate the promises of STAP for underwater surveillance purposes, models with varying characteristics and real data hence have to be used.

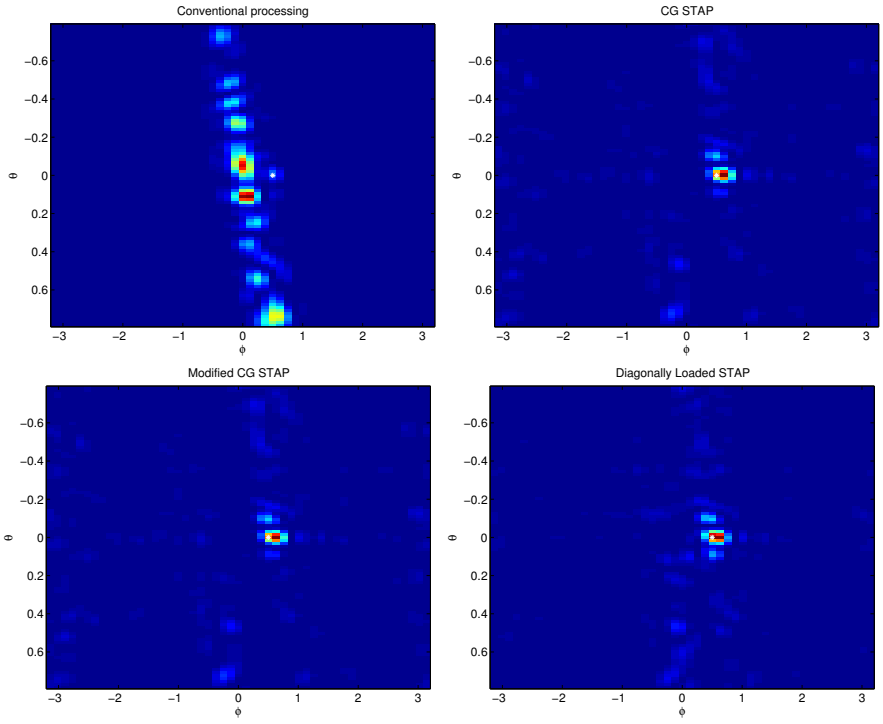

Figure 3.4: Performance for data obtained through Ray-tracing. From From left to right and top to bottom (a)-(d): (a) Angle-Doppler spectrum for the conventional processor. (b) Angle-Doppler spectrum for CG-STAP.(c) Angle-Doppler spectrum for MCG-STAP. (d) Angle-Doppler spectrum for diagonally loaded STAP.The true position of the target is indicated using the white mark.

Emitted pulse	Carrier frequency: $25\,kHz$ (CW) Pulselength: $0.02\,s$ Source level: $200\,dB$ re $1\,\mu Pa$@$1\,m$
Environment	Waterdepth: $60\,m$ Sound propagation: Upwards refracting winter profile with linear gradient from $1422\,m/s$ at the surface to $1425\,m/s$ at the bottom. Bottom properties: The upper layer has properties typical of a clay bottom with a density of $1600\,kg/m^3$. Sound velocity increases with depth from $1435\,m/s$ till $1740\,m/s$. Total reflection for grazing angles less than 7^o. Surface properties: Total reflection

Table 3.1: Specification of transmitted pulse and underwater environment.

4 Synthetic Aperture Sonar (SAS) Processing

In synthetic aperture sonar (SAS) processing coherent integration of echoes from several pings is used to improve the detection and resolution in the sonar image. As pointed out by Cutrona in 1975 [34] the main attractive property of SAS processing is that the azimuthal (along-track) resolution achievable under ideal conditions is *independent of target range*. This simple result is obtained by noting that the azimuthal beamwidth at SAS-processing of data from a linear synthetic aperture with length L_{sa} is [34, Eqn (2)]

$$\beta_{sa} \;=\; \frac{\lambda}{2L_{sa}} \tag{4.1}$$

radians, where λ is the wavelength. Assuming that the distance from the target to the sonar track is D and that the synthetic processing uses all pings along the track for which the target is inside the emitter lobe, the length of the synthetic aperture is

$$L_{sa} \;=\; 2D\tan\frac{\beta_e}{2} \tag{4.2}$$

where β_e is the horizontal width (in radians) of the emitter lobe. By combining equations (4.1) and (4.2) the along-track resolution at the target is seen to be

$$\Delta x_{sa} \;=\; D\beta_{sa} \;=\; \frac{\lambda}{4\tan(\beta_e/2)} \tag{4.3}$$

which is independent of the range D to the target. In contrast, the beamwidth at conventional sonar processing is

$$\beta_c \;=\; \frac{\lambda}{L} \tag{4.4}$$

where L is the physical aperture of the receiver array, and the along-track resolution cell of conventional processing is

$$\Delta x_c \;=\; D\beta_c \;=\; \frac{D\lambda}{L} \tag{4.5}$$

and thus grows linearly with target range D.

As seen from equation (4.4) the beamwidth of a conventional linear array with length L_{sa} would be twice the SAS beamwidth (4.1), which illustrates that SAS and conventional beamforming are closely related. The factor two arises since with a conventional array the emitter is fixed, e.g. at the center of the array, while in SAS the emitter moves along the array which approximatively doubles the variation of the source → target → receiver travel time as function of receiver position [34], [35].

The range resolution, achieved by replica correlation processing, is

$$\Delta y_{sa} \;=\; \Delta y_c \;=\; \frac{c\Delta t}{2} \tag{4.6}$$

for both SAS and conventional sonar, where c and Δt are the soundspeed and the 3dB width of the autocorrelation of the emitted waveform. For an LFM pulse with center frequency f_c, bandwitdh B and length T

$$s(t) \;=\; f_c t \;+\; \frac{Bt^2}{2T} \qquad -\frac{T}{2} \;\le\; t \;\le\; \frac{T}{2} \tag{4.7}$$

the autocorrelation width is approximately

$$\Delta t \approx \frac{1}{B} \tag{4.8}$$

The range resolution is then

$$\Delta y_{sa} = \Delta y_c \approx \frac{c}{2B} \tag{4.9}$$

obtained from equations (4.6) and (4.8).

It should be noted that equation (4.3) is derived assuming an ideal propagation medium, and that the resolution achievable by SAS will in practice be reduced by complications such as multipath propagation and incomplete or imprecise information on the acoustic parameters of the underwater medium as well as on the position and orientation of the sonar. The purpose of the simulations presented here is to investigate the effect of such complications on the SAS processing.

4.1 Surveillance scenarios

The parameters of the simulations presented below are chosen to be representative for surveillance with a variable depth sonar (VDS) towed by a surface-ship. The sonar has a 60° horizontal emitter lobe and a 87 cm long linear uniform array of 16 receiver hydrophones. The emitted waveform is a 20 ms long LFM pulse with center frequency 25 kHz and bandwidth 5 kHz.

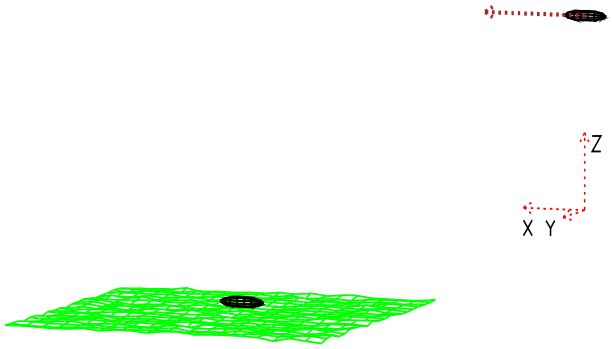

Figure 4.1: SAS surveillance scenario.

A shallow-water surveillance scenario is considered, with a target close to the seafloor and the sonar at depth 5 m. Figure 4.1 illustrates the surveillance scenario, showing the towed sonar platform with its trajectory indicated by an arrow, the seafloor and a the target located near the seafloor. The target, shown in figure 4.2, is a simplistic model of the Kongsberg HUGIN 1000 AUV [36]. It is a rigid (acoustically impenetrable) rotationally symmetric body with a convex smooth surface with overall length 406 cm and maximal diameter 76 cm. The lengths of the conical nose and tail sections are 125 cm and 116 cm. The target AUV is positioned near the seafloor at (horizontal) range 300 m from the trajectory of the sonar. The orientation of the AUV is parallel to the sonar trajectory, i.e. the AUV shows its broadside towards the sonar

4.2 The SAFIX model

SAFIX is a tool for modelling and analysis of underwater acoustic surveillance using a moving platform and SAS processing. This section gives a brief

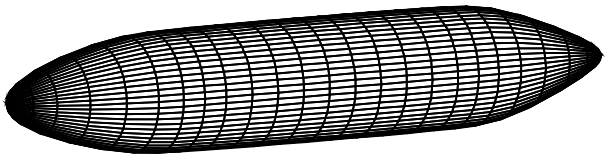

Figure 4.2: Computational model of the HUGIN 1000 AUV. Length: 406 cm, Max diameter 76 cm.

overview of the components of SAFIX used in the simulations below.

4.2.1 Underwater medium

The medium is modelled as a range-independent water layer, with piecewise constant soundspeed as function of depth. The water surface is perfectly reflecting sound soft (reflection coefficient $R = -1$), the seafloor is perfectly reflecting sound hard ($R = 1$) and reverberant, with reverberation modelled by point scatterers as described in 4.2.3 below.

4.2.2 Sound propagation and target scattering

The emitter is treated as a point source, and sound propagation is modelled by acoustic ray theory [33, Ch. 3]. The sound speed in the water is modelled as a piecewise constant function of depth z only. Thus each ray path is polygonal with corners at the boundaries $z = z_j$ $j = 1, ..., N$ of the homogeneous water layers and at the surface of the 3D target. A ray path composed of K linear segments is then described by a $2(K-1)$-dimensional vector $\boldsymbol{P}$ of coordinates of the corners on their respective 2D surface. Eigenrays are computed by minimizing sound travel time $T(\boldsymbol{P})$ along the ray as function of $\boldsymbol{P}$. $T(\boldsymbol{P})$ is a nonlinear function with a band-structured second derivative matrix, and the minimization problem can be solved efficiently using a trust region method [37] that makes use of the first and second derivatives of $T(\boldsymbol{P})$. Figure 4.3 illustrates this modelling by showing two types of eigenrays in a ten-layer water column approximating a linearly decreasing sound speed with depth. The eigenray types are source - target - receiver and source - target - water surface - receiver, respectively.
The transfer function $H_j(f)$ from source to receiver j is obtained as the sum of contributions from eigenrays of the K selected types

$$H_j(f) \;=\; \sum_{k=1}^{K} H_{kj}(f) \;=\; \sum_{k=1}^{K} \alpha_{kj}\;\; e^{i2\pi f \tau_{kj}} \tag{4.10}$$

where τ_{kj} is the travel time along ray k and α_{kj} accounts for the amplitude and phase change induced by change of ray tube area, sound absorption in the volume, reflections at the target, the surface and the bottom, and passage of caustic points. The contribution to α_{kj} from a reflection at the target, the surface or the bottom is modelled by a local plane-wave reflection coefficient and by the change of the derivative of the ray tube area w.r.t. the launch angles induced by the reflection. At target reflections, the change of the derivatives of the ray tube area is a function of the incidence angle and the two principal radii of curvature of the target surface at the reflection point.

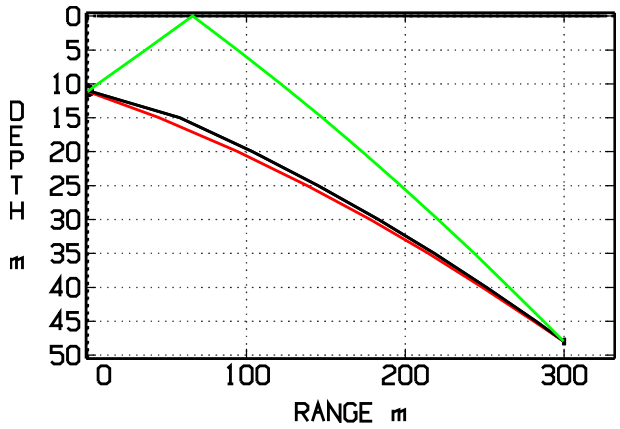

Figure 4.3: Two types of eigenrays: Source - target - receiver and source - target - water surface - receiver, with the parts after target reflection in red and green, respectively.

4.2.3 Bottom reverberation

Bottom reverberation is modelled as the sum of echoes from a large number M of point reflectors with random strengths Q_m and locations $\boldsymbol{r}_m$, $m = 1, ..., M$ on the seafloor. Neglecting sound speed variations and multipath propagation, bottom reverberation contributes to the field at receiver j with

$$P_j^l(t) = \sum_{m=1}^{M} Q_m \frac{s(t-\tau_{jm})}{R_{jm}R_m} \tag{4.11}$$

where R_{jm} and R_m are the distances from point scatterer m to receiver j and to the source, respectively, and

$$\tau_{jm} = \frac{R_{jm}+R_m}{c} \tag{4.12}$$

is the travel time from the source to point scatterer m to receiver j. The strengths Q_m of the point reflectors are stochastically independent random numbers uniformly distributed in $[0, q]$. The constant q is chosen so that the total energy E_s of the sound backscattered to the source is consistent with Lambert's law, stating that the intensity dI_s as function of scattering angle θ_s of sound scattered by a bottom patch with area dA is

$$dI_s = \mu I_i \sin(\theta_i)\sin(\theta_s)dA \tag{4.13}$$

I_i and θ_i are the intensity and the grazing angle of the incident sound, and μ is Lambert's scattering constant, representing the roughness of the seafloor and the materials and structures below.

From (4.13) follows, assuming the seafloor to be horizontal,

$$E_s \approx \frac{1}{2}E_e\mu\beta_e c\int_{t0}^{t1}\frac{\sin^2\theta(t)}{R(t)^3}dt \tag{4.14}$$

where E_e is the energy of the emitted pulse 1 m away from the source, β_e the horizontal width of the emitter lobe, and t_0, t_1 the minimal and maximal two-way travel times to the bottom rectangle selected for SAS imaging. $R(t)$ and $\theta(t)$ are the length and the grazing angle of the ray for which the two-way travel time to the seafloor is t.

4.2.4 Target shadows

A useful feature of SAS, analoguous to conventional high-resolution systems such as side-scan and mine-hunting sonars, is that regions of the seafloor shadowed by targets give rize to shadows in the SAS image of the bottom reverberation. Such shadows provide a means of detecting targets near the seafloor with target-strength to reverberation-level too small for detection using the physical aperture of the sonar only. Furthermore, the shapes of the shadows have the high resolution achieved by the SAS processing, and can therefore be used for target identification.

In SAFIX, target shadows in the bottom reverberation are modelled by computing, for each target, the boundary of its shadow on the seafloor and excluding points inside the boundary from the sum (4.11).

4.2.5 SAS image integration

The SAS image is defined by a grid of pixel points $(x_k, y_k, z_k)\ \ k = 1, ..., L$ covering the area of the seafloor selected for SAS imaging, together with complex pixel values F_k associated with the pixel points. All pixel values are initially zero, and are subsequently updated after each ping by beamforming focused at the pixel points. The image updates are obtained by 'back projection' processing, comprised of five steps:

1. The received signals $p_i(t)\ \ i = 1, ..., K$ are sampled at time-points covering the interval of two-way propagation times to the pixel points. Their Fourier spectra $\hat{p}_i(f)\ \ i = 1, ..., K$ are computed by FFT.

2. The Fourier spectra of the correlations $p_i^c(t)\ \ i = 1, ..., K$ of the signals $p_i(t)\ \ i = 1, ..., K$ with the emitted pulse $s(t)$ are computed as the product of the Fourier spectrum $\hat{s}(f)$ and $\hat{p}_i(f)\ \ i = 1, ..., K$.

3. The (complex-valued) analytic signals $p_i^a(t)\ \ i = 1, ..., K$ are computed by inverse FFT of the one-sided spectra of $p_i^c(t)\ \ i = 1, ..., K$.

4. Coefficients of B-spline expansions $\tilde{p}_i^a(t)\ \ i = 1, ..., K$ that interpolate to $p_i^a(t)\ \ i = 1, ..., K$ on $t_1, ..., t_n$ are computed from a linear system of equations with band structure and K right-hand-sides. The computational work for assembling and solving the linear system is $O(nK)$.

5. The pixel values $F_k\ \ k = 1, ..., L$ are incremented by

$$\Delta F_k \ = \ \sum_{i=1}^{K} \tilde{p}_i^a(\tau_{ik}) \tag{4.15}$$

where τ_{ik} is the source to pixel-point k to receiver i propagation time.

4.3 Simulations

The soundspeed in water is assumed to be 1430 m/s, the cross-track (range) resolution is then, by equation (4.9), $\Delta y \approx \frac{c}{2B} = 0.145$ m. Reverberation is modelled by incoherent bottom scattering according to equations (4.11) - (4.14), with Lambert's scattering constant set to $10 \log_{10} \mu = -15$.

The sonar moves along a 10 m long track, with such vessel speed and ping repetition frequency that the ping-to-ping movement of the vessel is half the length of the physical aperture. The target is located close to the seafloor, in the midpoint normal plane of the sonar track. The size of the SAS image area is 20 m $\times$ 20 m with pixel cell size 10 cm $\times$ 10 cm.

4.3.1 Ideal conditions

Figure 4.4 illustrates SAS processing in the idealized case of a homogeneous water column with soundspeed 1430 m/s, equal to the value assumed in the processing. The sound propagation occurs along the direct path only, i.e. interfering reflections from the surface and the bottom are neglected, and the position and orientation of the sonar are assumed to be exactly known.

The four frames show the pixel values $|F_k|$ in dB as function of (x, y) in a 20 m $\times$ 20 m area of the seafloor, after processing of data from 1, 8, 16, and 24 pings, respectively, along the 10 m long trajectory. The corresponding synthetic aperture lengths are 0.9 m, 3.9 m, 7.4 m, 10.9 m, and the corresponding along-track (azimuth) resolutions Δx expected by equations (4.1) - (4.5) are 10.0 m, 2.2 m, 1.2 m, 0.8 m.

The target shadow is invisible in the SAS image after ping 1 where only the physical aperture has been used, and emerges when the along-track resolution length Δx has decreased below ca 4 m, the along-track length of the target. Here the shadow is clearly recognizable after ping 8, and then becomes successively sharper. The cross-track extent of the shadow, ca 5 m, is in agreement with the diameter of the AUV and the grazing angle of the incident sound.

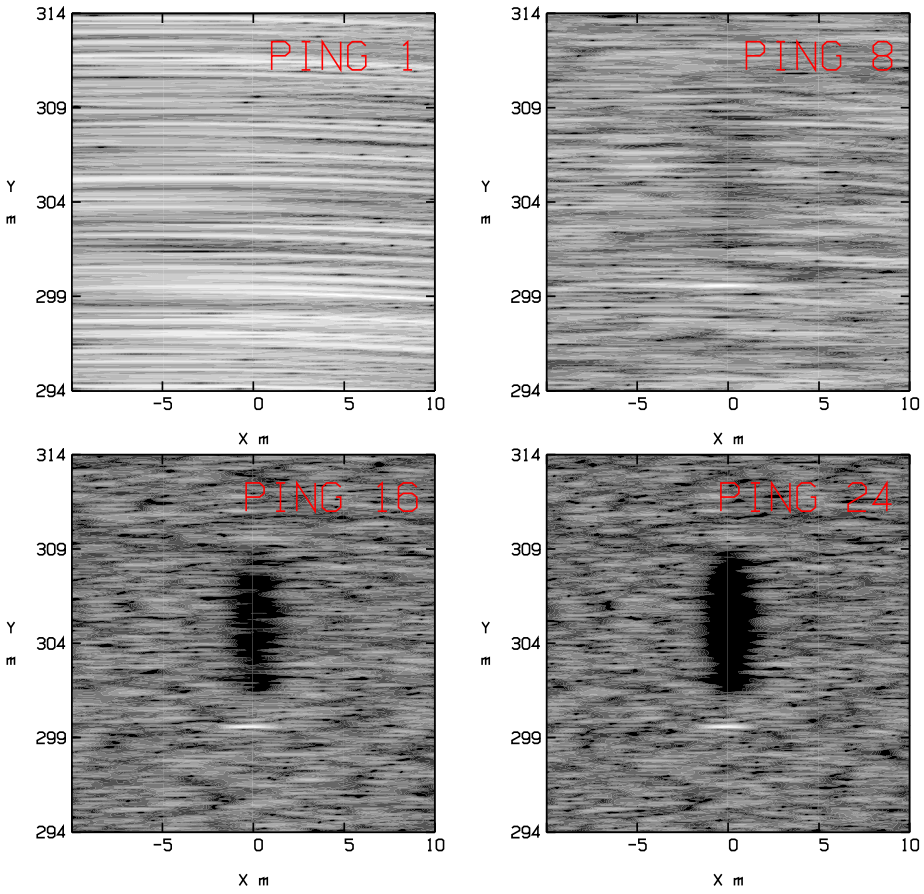

Figure 4.4: SAS processing under ideal conditions. Target range 300 m, target depth 49.5 m, water depth 50 m, aperture lengths 0.9 m, 3.9 m, 7.4 m and 10.9 m.

4.3.2 Effects of soundspeed variations and navigation data errors

In practice surveillance conditions are less well-defined than in the ideal case considered in Section 4.3.1. The performance of SAS procesing is influenced by spatial and temporal variations of the soundspeed, multipath propagation induced by reflections at the surface or the bottom and errors in the data on the position and orientation of the sonar (navigation data). This section presents some preliminary results from an investigation of such effects by simulations in which deviations from the ideal case are introduced in a well known way.

Figure 4.5 illustrates the influence of random errors in the sonar yaw angle data on the SAS image after ping 24, i.e. with synthetic aperture length 10.9 m as in the lower right frame of figure 4.4. All scenario parameters are the same as in the ideal case shown in figure 4.4, except for the yaw angle of the sonar which deviates randomly and uncorrelatedly from ping to ping around the value zero assumed in the SAS processing.

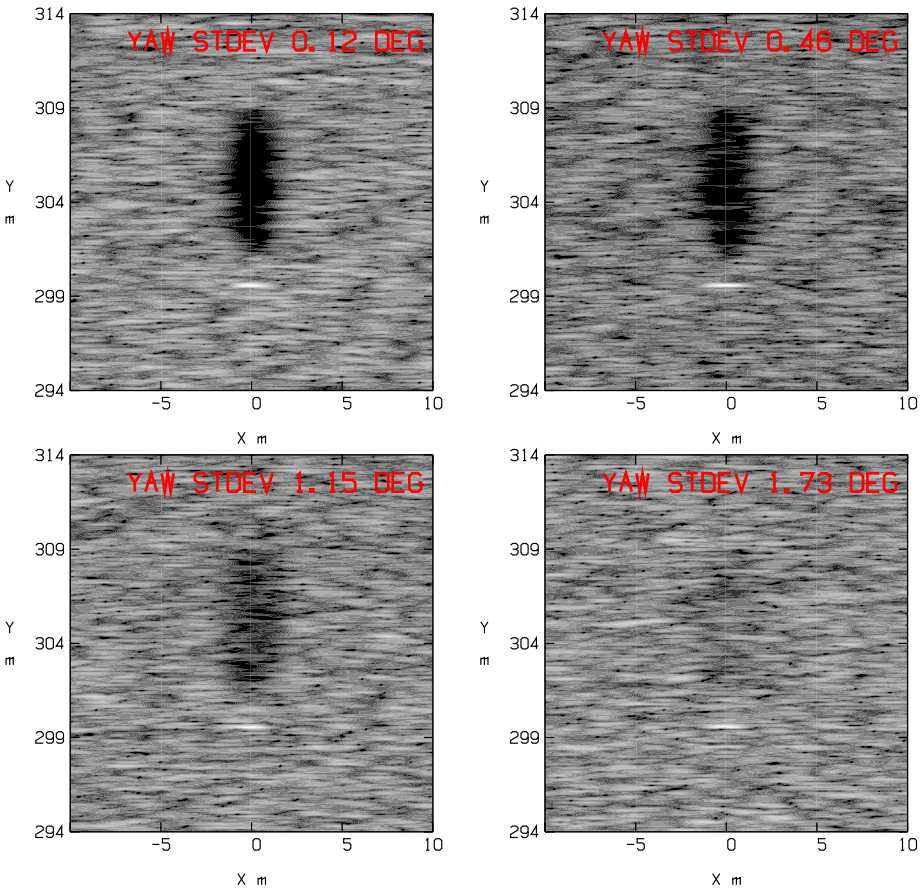

Figure 4.5: Influence of sonar yaw angle error on the SAS image in the lower right-hand frame of figure 4.4.

A random yaw-angle error with standard deviation $\Delta\phi$ induces a random error into the along-track coordinate (the x coordinate) of the updates of the SAS image. The standard deviation of this error is approximately

$$\Delta x = y\Delta\phi$$

where $y = 300$ m is the target range. In the four frames of figure 4.5 Δx is 1.0 m, 4.0 m, 8.4 m and 15.2 m, respectively, causing a corresponding loss of resolution in the SAS image. It is interesting to note, however, that both the target and the shadow are vaguely visible also in the lower right frame (standard deviation $\Delta\phi = 1.73°$), as opposed the upper left frame of figure 4.4 where data from a single ping only was used.

The effect on the SAS image of random variations of the sound speed is illustrated in figure 4.7. The water column is modelled as ten homogeneous layers, of varying thickness and sound speeds

$$c_j \;=\; \overline{c} + \delta_j \;\; j = 1, ..., 10$$

$\overline{c} = 1430$ m/s is the sound speed assumed in the SAS processing, and $\delta_j, j = 1, ..., 10$ are uncorrelated zero-mean random sound speed increments. In the cases shown in figure 4.7 these increments were not updated between pings, i.e. the soundspeed is modelled to vary randomly with depth with a correlation length of ca 3-4 m, and with time on a time-scale longer than the duration of the SAS run. The layer structure of the medium is shown in 4.6, together with an example of the non-linear sound propagation paths obtained with the standard deviation of the sound speed increments equal to 11.55 m/s.

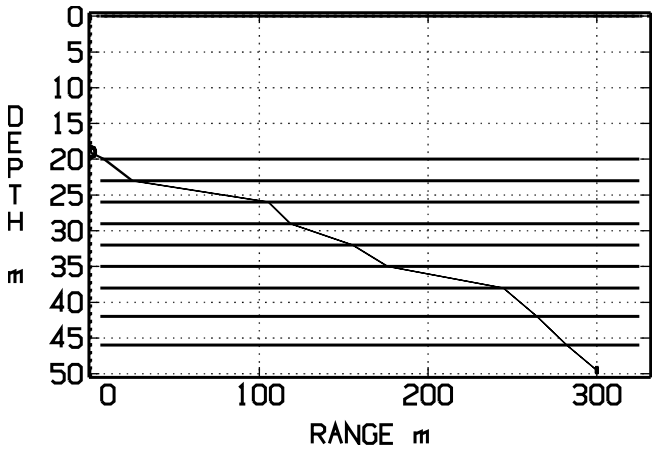

Figure 4.6: Rays from source to target to receiver in a water column with random variations of the soundspeed as function of depth.

The effects of such sound speed variations are seen from figure 4.7 to be reduction of both the along-track and the cross-track resolutions, and possibly (depending on the average soundspeed along the propagation paths) a displacement of the target in range. The degradation of the cross-track resolution with increasing variance of the sound speed increments causes the target echo to be lost in the lower right frame, whereas the target shadow remains clearly visible in all frames due to its longer cross-track length.

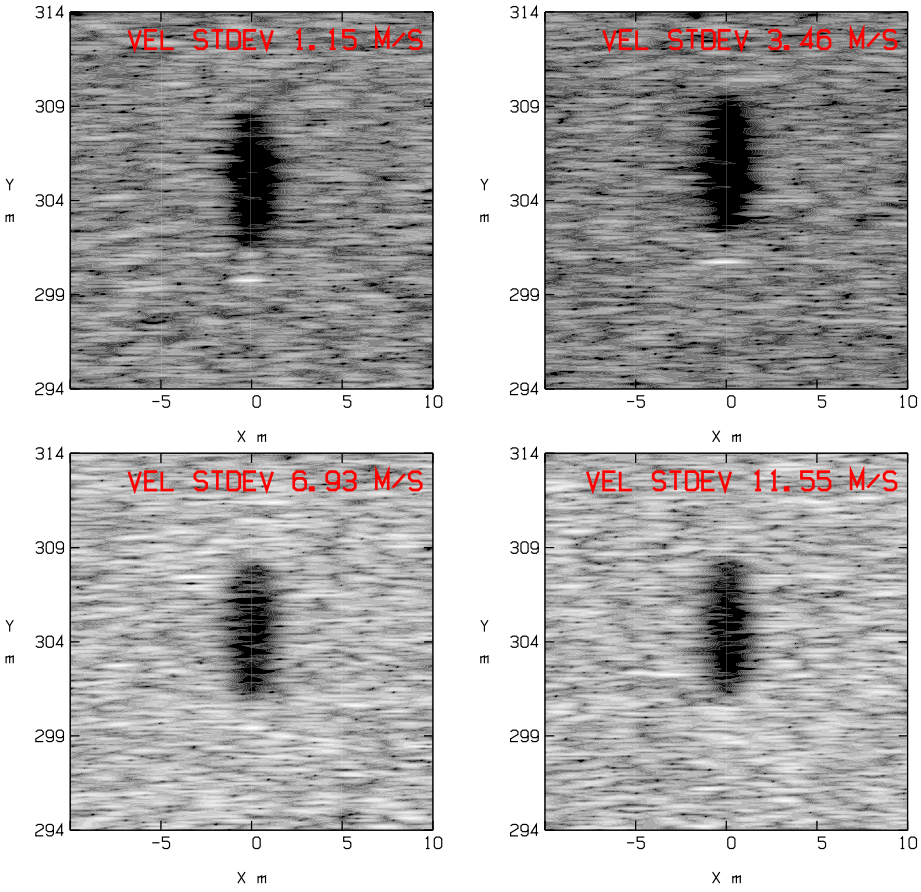

Figure 4.7: Influence of random variations in the sound speed as function of depth on the SAS image in the lower right-hand frame of figure 4.4.

5 Conclusions

Several sonar processing methods with a focus on reverberation-limited undersea environments have been investigated in this report.

Firstly, two methods for whitening of reverberation noise have been studied using simulated and sea trial data. In the first method the matched filter receiver was tuned for each range-bin using an estimate of the reverberation covariance matrix, and the tuned filter was subsequently applied to the following range-bin. It was shown to provide slightly better detection performance on a set of simulated data, but at a very large cost in the form of calculations. The second method was based on autoregressive (AR) modelling of the reverberation noise in a range-bin, and – similarly – the AR coefficients were then used to whiten the reverberation in a following range-bin. The AR modelling was applied to experiment data from the BAROC sea trial of 2002. Detection performance was improved significantly using the AR whitening, and it was achieved at a fairly low computational cost.

Secondly, the overall performance of the investigated STAP algorithms were very inspiring. Especially the derived *modified conjugate gradient* approach is very attractive since it seems to offer good adaptive performance with complexity in parity with that of the conventional processor. To further investigate the possibility of using this technique for underwater surveillance purposes it is necessary to explore real data to identify over how many adjacent range-bins the interference properties can be considered stationary. To further improve the reverberation mitigation, it would also be of interest to study means to incorporate prior knowledge, obtained from physical models, into the estimation of the interference covariance matrix, see [21].

Finally the simulation study undertaken here indicates that SAS processing under ideal conditions improves the target detection and identification performance of mobile active sonars such as a 25 kHz VDS. The improved performance arises from the high azimuthal resolution achievable with SAS, enabling more accurate and informative mapping of the surveyed scene, including higher resolution of multiple targets, detection of target shadows in the bottom reverberation, and resolution of the shapes of such shadows.

Under less idealized conditions the performance of SAS deteriorates due to errors in sonar navigation data, unknown variations of the soundspeed as function of range and depth, and other environmental effects such as multipath propagation and reflections from the surface and the bottom. The limited simulation results presented here suggest, however, that SAS processing can to some degree improve surveillance performance also in the presence of such complications. A more extensive simulation study would therefore be highly motivated, with the purpose to quantify the applicability of long-range low-frequency SAS in terms of parameters of the sonar, the navigation system and the environment.

References

[1] T. G. Kincaid. On optimum waveforms for correlation detection in the sonar environment: Reverberation-limited conditions. *Jornal of the Acoustical Society of America*, 44(3):787–796, September 1968.

[2] G. Jourdain and J. P. Henrioux. Use of large bandwidth-duration binary phase shift keying signals in target delay doppler measurements. *Journal of the Acoustical Society of America*, 90(1):299–309, 1991.

[3] Y. Doisy, L. Deruaz, S. P. Beerens, and R. Been. Target döppler estimation using wideband frequency modulated signals. *IEEE Transactions on Signal Processing*, 48(5), May 2000.

[4] E. Dalberg, L. Frenje, S. Ivansson, and B. Nilsson. Measurements and modelling of shallow water reverberation. Methodology Report FOA-R–00-01751-409–SE, Swedish Defence Research Agency, December 2000.

[5] J. Pihl, S. Ivansson, P. Karlsson, R. Lennartsson, M. Levonen, P. Morén, B. Nilsson, M. Olsson, Ö. Staaf, G. Sundin, and P. Söderberg. Low frequency active sonar – reverberation and performance in the baltic. Base Data Report FOI-R–0887–SE, Swedish Defence Research Agency, June 2003.

[6] R. O. Nielsen. *Sonar Signal Processing*. Artech House Books, 1991.

[7] R. N. McDonough and A. D. Whalen. *Detection of Signals in Noise*. Academic Press, Inc., Orlando, FL, USA, 1995.

[8] S. Kay. Optimal signal design for detection of gaussian point targets in stationary gaussian clutter/reverberation. *IEEE Journal of Selected Topics in Signal Processing*, 1(1):31–41, June 2007.

[9] L. Riddle. Properties of active sonar matched filtering. http://cnx.org/content/m14745, 2007.

[10] S. Kay and J. Salisbury. Improved active sonar detection using autoregressive prewhiteners. *Jornal of the Acoustical Society of America*, 87(4):1603–1611, April 1990.

[11] G. Ginolhac and G. Jourdain. Detection in presence of reverberation. In *Proceedings of Oceans 2000*, 2000.

[12] R. Klemm. *Space-Time Adaptive Processing: Principles and Applications*. IEE Press, London, 1998.

[13] A. Cederholm, M. Jönsson, I. Karasalo, P. Karlsson, S. Lindström, J. Pihl, J. Robinson, and E. Parastates. Högupplösande sensor under vatten. Teknisk rapport FOI-RH-0358, Swedish Defence Research Agency, December 2004.

[14] H. L. Van Trees. *Detection, Estimation, and Modulation Theory, Part I*. John Wiley & Sons Inc., USA, 2001.

[15] M. Lundberg. *Land Mine Detection using Dual-Band Electro-Optical Sensing*. PhD thesis, Chalmers University of Technology, 2003.

[16] G. Ginolhac and G. Jourdain. "Principal Component Inverse" Algorithm for Detection in the Presence of Reverberation. *IEEE Journal of Oceanic Engineering*, 27(2):310–321, April 2002.

[17] B. L. Andersson and I. Karasalo. Modeling of low-frequency sound propagation in the baltic. Base Data Report FOI-R–0875–SE, Swedish Defence Research Agency, June 2003.

[18] L. Brennan and I. Reed. Theory of adaptive radar. *IEEE Transactions on Aerospace and Electronic Systems*, 9(2):237–252, Mar 1973.

[19] B. Nilsson, P. A. Karlsson, I. Karasalo, M. Lundberg Nordenvaad, and E. Parastates. Active sonar methods – bistatic sonar, synthetic aperture sonar and space-time adaptive processing. Teknisk rapport FOI–R–2407, Swedish Defence Research Agency, November 2007.

[20] J. Ward. Space-time adaptive processing for airborne radar. Technical Report 1015, MIT Lincoln Laboratory, December 1994.

[21] O. Besson, S. Bidon, and J. Y. Tourneret. Covariance matrix estimation with heterogeneous samples. *IEEE Transactions on Signal Processing*, Accepted for Publication.

[22] B. D. Carlson. Covariance matrix estimation errors and diagonal loading in adaptive arrays. *IEEE Transactions on Aerospace and Electronic Systems*, 24(4), Jul 1988.

[23] H. L. Van Trees. *Optimum array processing, part IV of detection, estimation, and modulation theory.* John Wiley & Sons Inc., 2002.

[24] P. Stoica and J. Li. *Robust Adaptive Beamforming.* Wiley-Interscience, 2005.

[25] L. Svensson and M. Lundberg. On posterior distributions for signals in gaussian noise with unknown covariance. *IEEE Transactions on Signal Processing*, 53(9):3554–3571, Sept 2005.

[26] J. R. Guerci, J. S. Goldstein, and I. S. Reed. Optimal and adaptive reduced-rank stap. *IEEE Trans. on Aerospace and Electronic System*, 36(2), April 2000.

[27] J. S. Goldstein, I. S. Reed, and L. L. Scharf. A multistage representation of the wiener filter based on orthogonal projections. *IEEE Transactions on Information Theory*, 44(7):2943–2959, Nov 1998.

[28] M. R. Hestenes and E. Stiefel. Methods of conjugate gradients for solving linear systems. *J. Res. Nat. Bur. Stand*, 49, 1952.

[29] L. L. Scharf, E. K. P. Chong, M. D. Zoltowski, J. S. Goldsein, and I. S. Reed. Subspace expansion and the equivalence of conjugate direction and multistage wiener filters. *IEEE Transactions on Signal Processing*, 56(10), Oct 2008.

[30] H. Ge, L. L. Scharf, and M. Lundberg. Warp convergence in conjugate gradient wiener filters. In *2004 IEEE 5th Workshop on Signal Processing Advances in Wireless Communications*, July 2004.

[31] L. Abrahamsson. Raylab – a ray tracing program in underwater acoustics. Technical Report FOI-R–1047–SE, Swedish Defence Research Agency, 2003.

[32] L. Abrahamsson, N. Olofsson, and E. Parastates. Modellering av dopplerförskjutna signaler i rörlig målsökare. Technical Report FOI-RH–0433–SE, Swedish Defence Research Agency, 2005.

[33] M. B. Porter F. B. Jensen, W. A. Kuperman and H. Schmidt. *Computational ocean acoustics*. AIP Press, 1994.

[34] L. J. Cutrona. Comparison of sonar system performance achievable using synthetic-aperture techniques with the performance achievable by more conventional means. *Journal of the Acoustical Society of America*, 58(2):336–348, 1975.

[35] R. McHugh. The potential of synthetic aperture sonar in seafloor imaging. Technical Report CM 2000/T:12, Heriot-Watt University, Department of Computing and Electrical Engineering, Edinburgh, 2000.

[36] Hugin 1000, autonomous underwater vehicle (auv). Brochure, Kongsberg Simrad AS, Horten, Norway, http://www.km.kongsberg.com/, 2005.

[37] R. Fletcher. *Practical methods of optimization, Volume 1.* John Wiley, 1980.

FOI is an assignment-based authority under the Ministry of Defence. The core activities are research, method and technology development, as well as studies for the use of defence and security. The organization employs around 1000 people of whom around 800 are researchers. This makes FOI the largest research institute in Sweden. FOI provides its customers with leading expertise in a large number of fields such as security-policy studies and analyses in defence and security, assessment of different types of threats, systems for control and management of crises, protection against and management of hazardous substances, IT-security an the potential of new sensors.

FOI
Swedish Defence Research Agency
SE-164 90 STOCKHOLM

Tel: +46 8 5550 3000
Fax: +46 8 5550 3100

www.foi.se